50th AIAA Aerospace Sciences Meeting including the New Horizons Forum and Aerospace Exposition
09 - 12 January 2012, Nashville, Tennessee

AIAA 2012-0988

Electric Field Measurements in Gases Using Cavity Enhanced Polarimetry

Jordan Rath[1], Isaiah Franka[2], Brian Lee[3], Chris Hagen[4], Azer Yalin[5]
Colorado State University, Fort Collins, Colorado, 80523, USA

and

Mark Cappelli [6]
Stanford University, Palo Alto, California, 94305, USA

We report a novel form of cavity enhanced polarimetry to make electrical field measurements in gases via the optical Kerr effect. The measurement system uses a distributed feedback laser at 1742 nm as the light source and an optical cavity with finesse of 170,000. Electrical field measurements are made in gases between two parallel plates. The high finesse of the optical cavity provides higher sensitivity as compared to past measurements using single- or multi-pass cells. Measurements are presented for carbon dioxide, nitrogen, oxygen, and air. Experimental results are compared against model predictions based on published Kerr constants. Effects of laser linewidth (phase noise) and the experimental detection limit are discussed.

Nomenclature

B	=	optical Kerr coefficient (wavelength-dependent)
E	=	electric field strength
E_{in}	=	input electric field of laser beam to cavity
F	=	finesse
I_i	=	incident light intensity
I_0	=	light intensity transmitted through nulled analyzer
K	=	optical Kerr coefficient (wavelength-independent)
L	=	path length over which electric field is applied
L_0	=	optical path length (physical length of cavity)
L_{eff}	=	effective optical path length of high finesse cavity
$n_\perp$	=	refractive indexes along the directions perpendicular to electric field
$n_{\|\|}$	=	refractive index along the direction parallel to electric field
R	=	mirror reflectivity
T	=	mirror transmission
t	=	time
τ_{cav}	=	cavity ring-down time
x	=	position along the optical axis within the cavity
λ	=	optical wavelength
ω_0	=	laser frequency
θ_K	=	phase difference
Δn	=	difference of refractive indexes along directions parallel and perpendicular to electric field

[1] Graduate Research Associate, Department of Mechanical Engineering
[2] Graduate Research Associate, Department of Mechanical Engineering
[3] Graduate Research Associate, Department of Physics
[4] Research Scientist, Department of Mechanical Engineering
[5] Associate Professor, Department of Mechanical Engineering, AIAA Senior Member
[6] Professor, Department of Mechanical Engineering, AIAA Member

I. Introduction

There are few methods for non-invasive measurements of the electric field in non-radiating gases. A method which has been used with some success is based on the optical Kerr effect (see for example general discussion by Buckingham and Dunmur [1]), which takes advantage of the electric-field induced linear birefringence (i.e. different indexes of refraction for different linear polarizations). Early work has examined the Kerr effect in gases at high pressures (~10-100 bar) for which the induced birefringence is relatively strong [2, 3]. Often, a linear dependence of the Kerr constant on number density is assumed in order to extrapolate to lower pressures and estimate the birefringence at ambient conditions. More recent work, summarized below, has used sensitive optical techniques to study the Kerr effect at lower pressures including atmospheric pressure.

One recent experiment has directly measured the Kerr constant of air at ambient conditions, in a laser multi-pass configuration [4]. The path length used in that study was 13 m. Here, we describe a potentially more sensitive method, which may allow spatially-resolved measurements of moderate electric fields (~1-10 kV/cm) over small distances. We make use of the enhanced cavity length provided by a high-finesse optical cavity to accumulate the Kerr induced phase rotation over longer path lengths. Similar to cavity ring-down spectroscopy (CRDS), we exploit the large effective path-length provided by the successive reflections of optical radiation inside an optical cavity comprised of two highly reflective mirrors. As will be further discussed below, for mirror reflectivity of R=0.9999, one has a cavity finesse of approximately 30,000 and a path length enhancement of approximately 20,000 (in fact higher values are obtained in the present experiment).

Several experiments have employed cavity enhanced spectroscopy for measurement of birefringent effects. Circular birefringence (different indexes for left- and right-handed circularly polarized light) and circular dichroism (different losses for left- and right-handed circularly polarized light) have been studied via cavity ring-down polarimetry (CRDP) [5, 6]. In order to accumulate the polarization rotations (chiral effects) in a linear cavity, each of the cavity mirrors is preceded by a quarter wave plate (which allow for accumulation of the polarization effects, but also add loss to the cavity and lower the length enhancement). Engeln et al. have performed polarization dependent CRDS where the rate of absorption is measured and the polarization dependent loss is inferred [7]. Polarization dependent absorption spectra for oxygen molecules in the presence of magnetic fields were recorded. The same research group has also shown a cavity enhanced absorption spectroscopy (CEAS) configuration where time-integrated absorption signals (as opposed to ring-down signals) are measured [8].

While polarization rotation due to circular birefringence does not accumulate over multiple passes in a linear cavity (unless lossy wave plates are introduced), effects of linear birefringence do accumulate. At first inspection this may not be obvious, since a medium with linear birefringence is equivalent to a wave plate, and wave plates are nominally reciprocal elements [9]. However, the reciprocity applies for phase conjugate beams, and in a cavity configuration the beam that re-enters the waveplate has undergone a reflection off the cavity mirror which does not provide a phase-conjugate. (This is true for both metal and dielectric cavity mirrors, and is also very analogous to laser Q-switch configurations where the double passage through a quarter wave plate Pockels cell, after reflection off of a cavity reflector, causes a net polarization rotation of half a period.) Indeed, the cavity enhanced Kerr effect has been studied using linear cavities. Bielsa et al. studied the Kerr effect of molecular oxygen by locking a laser beam to a ring-cavity [10]. The electric field was modulated and a homodyne technique was used to measure the Kerr induced phase change. The closest work to ours is that of Inbar et al., who also used a laser locked cavity to enhance the phase change and who made measurements of the Kerr effect for CO_2, N_2, and O_2 at atmospheric pressure [11]. A key difference in our configuration is that we do not use an actively locked cavity so that our system is less technically demanding and potentially more amenable to implementations, such as for probing harsh discharge plasmas, where field strengths are comparable to those measured here and where cavity locking may be difficult. In past studies, electric fields in discharge plasmas have been made from measurements of emission [12] or from laser-induced fluorescence from excited states [13]. Finally, we mention that the Cotton-Mouton effect, i.e. magnetically induced linear birefringence, has also been studied with related cavity enhanced schemes [14, 15].

In this contribution we perform Kerr effect field measurements via cavity enhanced polarimetry. In Section II we present the basic theory of the Kerr effect and present a simple framework for signal analysis based on summing the passes of the beam within the cavity and birefringent medium. The experimental setup based on a high-finesse 1742 nm ring-down system is described in Section III. Results and discussion are presented in Section IV including measurements for N_2, CO_2, O_2, and air at atmospheric pressure, comparison of the data against our model and published cross-sections, and discussion of sensitivity limitations imposed by the optical cavity technique. The

results show that our technique may be useful for applications such as mapping of the electric field surrounding wire to plane corona discharges, where fields can be much higher than ~1 kV/cm [16]. Conclusions are presented in Section V.

II. Theory

Electric-field induced (linear) birefringence is known as the Kerr effect. An applied static field affects the optical anisotropy of the medium through the difference, Δn, in the component of its refractive index along the direction parallel ($n_{\parallel}$) and perpendicular to the field ($n_{\perp}$):

$$\Delta n = n_{\parallel} - n_{\perp} \tag{1}$$

In electric birefringence, the optical Kerr constant [4], K, relates this difference to the static electric field strength, E:

$$\Delta n = \lambda K E^2 \tag{2}$$

where, λ is the wavelength. K is the wavelength-independent Kerr constant which is related to the wavelength-dependent Kerr constant, B, as $K=B\lambda/n$, where n is the index-of-refraction at λ (taken to be unity in this work as we are far from resonant transitions). In some cases, Kerr constants are expressed per unit number density, but more commonly the constants are reported for atmospheric pressure (with a linear scaling for number density) [17]. Numeric values of the Kerr constants for several gases are provided in Section III. The phase shift induced between light polarized parallel and perpendicular to the static field, after traversing a distance L across the uniform field, is given as:

$$\theta_K = 2\pi\Delta n L/\lambda = 2\pi K L E^2 \tag{3}$$

For ambient gases (e.g. N_2 and CO_2) in static fields of $E \sim 10^6$ V/m (=10 kV/cm), and over path lengths ~10 cm, the phase difference is on the order of micro-radians. The most straightforward measurement technique is to align the incident light at 45 degrees relative to the parallel and perpendicular field directions, and then to measure the light intensity through a nulled analyzer polarizer:

$$I_0/I_i = \sin^2\left(\theta_K/2\right) \tag{4}$$

where I_0 is the intensity transmitted through the nulled analyzer and I_i is the incident light intensity. For example, Kumada et al. have used this method but the smallest phase shift they could measure was 50 micro-radians per pass [4]. The cavity enhanced method that we employ extends the effective path length, L_{eff}, thus providing larger phase shifts. Owing to the multiple passes within the cavity, the effective path length is found as:

$$L_{eff} = 2FL_0/\pi \tag{5}$$

where L_0 is the actual cavity length, and F is the cavity finesse:

$$F = \pi\sqrt{R}/\left(1-R\right) \tag{6}$$

As a first approximation, the cavity enhanced signals that we measure can be analyzed using eqns (3) and (4) but considering that the effective length is enhanced by a factor of $2F/\pi$ (from eqn (5)). For typical mirror reflectivities of R = 99.99% (finesse of ~30,000), the enhancement factor is significant, i.e. approximately 20,000. The resulting phase shifts accumulated over the multiple cavity passes are then in the milli-radian range and more tractable for measurement.

In our experimental scheme, we scan the laser (with a triangular current ramp) such that it sequentially passes over multiple cavity resonances (i.e., cavity transmission peaks each separated by a free spectral range). As it crosses each resonance, light is coupled into the cavity and transmitted through the cavity. We measure, with crossed polarizers, the (temporally integrated) light due to each passage over a cavity resonance. The ratio of the crossed polarizer signals (parallel and perpendicular to the incident field) is dependent on the Kerr induced polarization rotation.

For fuller consideration of the behavior of light inside the cavity, and its birefringent effects, we perform an analysis of the temporal evolution of the optical signals and their polarization dependences. We use the infinite-sum approach of Morville et al. [18] to which we add birefringence. Equation (7) gives the time-dependence of the electric field components parallel and perpendicular to the electric field directions:

$$E_{\parallel}(x,t) = \sqrt{T}E_{in}(x,t)\sum_{m=0}^{\infty} R^m \exp\left(i\frac{2\omega_o}{c/n_{\parallel}}\left\{\left[L_o + v\left(t - \frac{x-L_o}{c/n_{\parallel}} \right)\right]m - \frac{v}{c/n_{\parallel}}L_o m^2 \right\}\right)$$
$$E_{\perp}(x,t) = \sqrt{T}E_{in}(x,t)\sum_{m=0}^{\infty} R^m \exp\left(i\frac{2\omega_o}{c/n_{\perp}}\left\{\left[L_o + v\left(t - \frac{x-L_o}{c/n_{\perp}} \right)\right]m - \frac{v}{c/n_{\perp}}L_o m^2 \right\}\right) \quad (7)$$

where $E_{\parallel}$ and $E_{\perp}$ are the parallel and perpendicular components respectively, T is the mirror transmission, x is position along the optical axis within the cavity, t is time, ω_0 is the laser frequency, L_0 is the cavity length, and v is the velocity of the moving cavity mirror (or the equivalent laser scan speed). In our model we take $n_{\perp}$=1 and $n_{\parallel} = n_{\perp}+\Delta n$, where Δn is computed from eqn. (2) but with a multiplicative factor of L/L_0 to reflect the fact that the parallel plate electrodes do not fill the full cavity. The resultant electric field in a given direction, e.g. along the direction of the polarizer analyzer, can be found from the vector components and the intensity (as measured by a photo-detector) as the magnitude squared.

As an example of the polarization rotation, Figure 1 shows modeled signals due to passage through the optical cavity calculated using eqn. (4). The modeled case assumes a Kerr constant of B=10^{-18} m/V^2 (typical of gases [17]), electric field magnitude of E = 10 kV/cm (giving Δn=1.7x10^{-12}), input electric field (polarizer) polarized at 45 degrees to the parallel and perpendicular field axes, and cavity parameters of our current system as described below (cavity length of 90 cm, and R=0.999982). The panel on the left shows the cavity output signal through an analyzer polarizer parallel to the input beam, while the panel on the right shows the cavity output signal through an orthogonal analyzer polarizer. The left panel is similar to a regular "ring-down trace" with a decay at roughly the 1/*e* time of the cavity, though in this case the laser is not extinguished by a modulator, rather the laser frequency is swept over the cavity resonance providing a natural extinction. The signal through the latter polarizer is due to the Kerr induced polarization rotation (the vertical axis has a different scale and only a relatively small fraction of light passes through this polarizer). Note that, because the phase of light in the cavity is continuously evolving, proportionally more light is transmitted through the nulled (orthogonal) polarizer at later time. Our measurement method is to measure the two signals shown in Figure 1 and to take the ratio of their areas, and then to use a model based on eqn. (7) to relate the area ratio to the applied field.

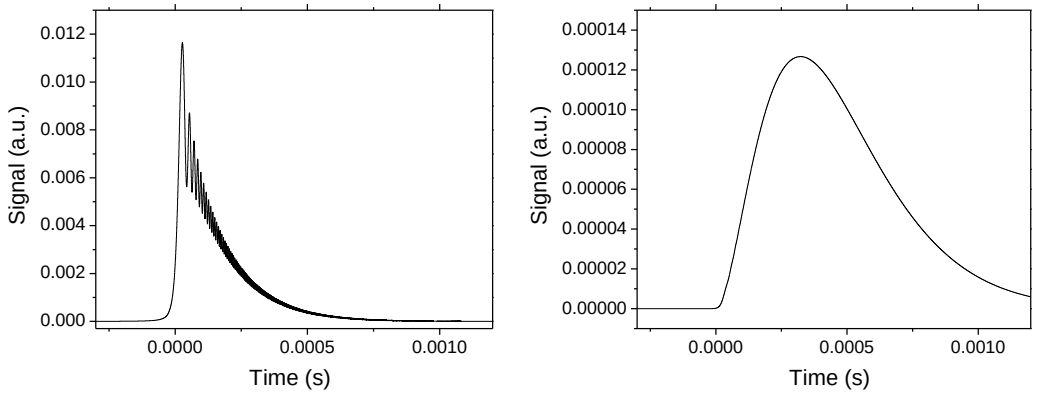

Figure 1. Left: Cavity output signal through an analyzer polarizer parallel to the input polarization. Right: Cavity output signal through an orthogonal analyzer polarizer.

As discussed below, our experimental scheme measures the light through both analyzer legs (parallel and perpendicular) as the laser is passed over a cavity resonance. We then ratio the areas of the two traces, e.g. for

conditions of Figure 1, the area of the trace through the perpendicular polarizer to that of the parallel polarizer is 0.047. Although we use an analyzer polarizer and a trigger circuit with fast detector, the basic measurement is analogous to CEAS (also referred to as integrated cavity output spectroscopy). This measurement configuration is in contrast to CRDS where the light entering the cavity is extinguished (or a short pulse is used) and the subsequent ring-down decay is measured. Engeln et al. have derived expressions for polarization dependent CRDS based on ring-down time constants and loss rates [5] but these expressions do not apply to our experiment because they assume that light in the cavity does not begin to accumulate (Kerr induced) phase change until the start of the decay (as would be the case if a short pulsed laser were used, or the applied field were turned on with a switch at the start of the ring-down time). In our experiment, in contrast, the applied field is present continuously and the phase change begin to accumulate as soon as light enters the cavity and continues to accumulate during the full time that the light is in the cavity and the laser passes over a cavity resonance.

III. Experimental

The cavity enhanced polarimeter is based on a continuous-wave (cw) CRDS setup at 1742 nm developed for sensitive detection of hydrogen chloride (HCl). We periodically operate in CRDS mode to measure the decay time and infer the mirror reflectivity (as it is needed in the analysis) but Kerr measurements are made by sweeping the laser over cavity resonances without extinguishing the beam. The system uses a commercially available distributed feedback (DFB) laser as the light source. The DFB lasers employ internal Bragg gratings to enable narrow linewidth single-frequency output and continuous (mode-hop free) tuning *without* the need for an external cavity. Therefore, the design is simpler and has fewer moving parts compared to an external cavity system in which the laser is tuned via a moving diffraction grating. The DFB laser we use (NEL model KELD1F5DAAA) has an output power of 15 mW, linewidth of ~5 MHz and a fiber coupled single-mode output. A schematic diagram of the optical aspects of the sensor is shown in Figure 2. The laser output is delivered to the optical cavity via several mirrors. The optical cavity has length of 90 cm and is formed by a pair of high reflectivity mirrors each 2.54 cm in diameter with reflectivity of 0.99998 (Advanced Thin Films). Simple beam-shaping optics (lens pair) are used to mode-match the beam to the cavity. During a typical experiment the laser is scanned (with a triangular current ramp) with a scan speed of 5.7 GHz/s over an extent of ~10 GHz such that it sequentially overlaps multiple cavity resonances. As described below, as the laser passes each resonance light is transmitted through the cavity and a trigger circuit (connected to the photodetector that monitors the parallel polarizer beam) is used to capture the signals through the two polarizers.

The applied electric field is created between a pair of parallel plates surrounding the cavity. The separation between the plates is 16 mm and they are connected to a high voltage DC power supply with applied voltages ranging from 0 to 18 kV. The sample gas flows slowly within a pyrex tube that itself is between the parallel plates. The pyrex tube is a dielectric that slightly alters the electric field. We have used a simple finite element solver and find that, for our geometry, the field in the tube is approximately 97% of the field found as the plate separation divided by the applied voltage (and we enter the fields into our model accordingly). We use a thin film polarizer (Thorlabs LPNIR050-MP) to set the light polarization prior to entering the cavity. The polarization is set to an angle of 45 degrees relative to the electric field direction. A second analyzer polarizer (Glan-Taylor Thorlabs GT10-C) is positioned behind the cavity and is aligned to its null position (orthogonal to the input polarization). The Kerr induced polarization rotation causes the input linear polarization to become slightly elliptical so that a small fraction of the beam is transmitted through the analyzer. The transmitted beam is measured with an extended-wavelength InGaAs photodetector (Hamamatsu, G8421-03) with transimpedance amplifier (Analog Modules, 341-1-INV-10pF). In order to trigger and detect this rather weak beam, and to normalize laser power fluctuations, we also detect the (stronger) beam that is rejected by the analyzer polarizer (polarization approximately parallel to the input polarizer) with a second detector (Thorlabs PDA10CS). The signals from both photodetectors are passed to a computer via an A/D board (National Instruments, PCI-6132). The beam that is rejected by the polarizer is used to trigger the acquisition of signals from both beams. A pre-trigger (1.67 ms) is used in order to capture waveforms from each detector similar to those shown in Fig. 1. The acquisition system averages multiple signals together (for each beam) as the laser passes repeatedly over the cavity resonance, and then fits an area (to the signal from each beam) and ratios these to one another.

To determine the ring-down time, we operate in CRDS mode (not shown in Fig. 2) by removing the analyzer polarizer and using the extended-wavelength InGaAs photodetector to measure ring-down decays. In this case a triggering circuit (connected to the photodetector) monitors the cavity transmission and, as soon as the transmitted

intensity reaches a pre-set threshold, triggers an acousto-optic modulator to extinguish the beam. The optical intensity within the cavity then decays (rings-down).

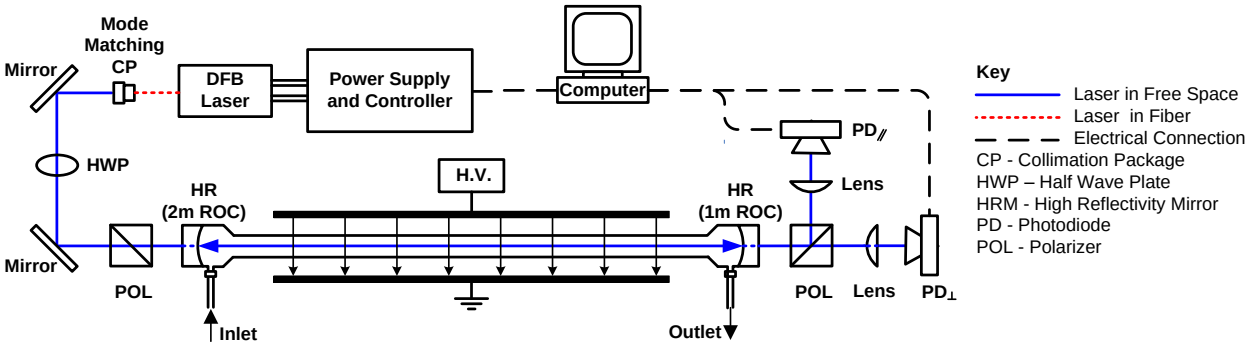

Figure 2. Schematic of cavity enhanced polarimeter with High Voltage plates.

IV. Results and Discussion

A. Observation of Kerr Induced Phase Shift and Temporal Traces

Here, we present results illustrating the measurement system and the Kerr induced phase shift. Figure 3 shows traces through both polarizers (i.e., through the nulled polarizer that is perpendicular to the incident field, and through the aligned polarizer that is parallel to the incident field) for zero field and applied field cases. The sample gas in the cell is CO_2 at atmospheric pressure (0.85 bar in Fort Collins, CO). The temporal traces correspond to the signals measured on the two detectors as the laser is swept over cavity resonances. Individual traces, particularly for the perpendicular analyzer, are rather weak and the traces shown are averages (accumulations) of 6000 shots. Owing to the amplitude fluctuations of the individual shots, and the trigger method (fixed threshold), the averaging serves to temporally smear the individual traces so that their temporal extent is considerably broader than that predicted by the model (e.g. the modeled traces of Figure 1).

We first consider the left plots where there is no applied field. In this case, there is no Kerr induced polarization rotation and so light leaving the cavity is predominantly parallel to the incident light. The signal on the parallel polarizer is therefore much larger than that of the perpendicular polarizer. The vertical scales for the two polarizers are different, owing to different detectors, but we have performed a calibration that shows that with zero field the total amount of light on the perpendicular polarizer is $1/400^{th}$ of the light on the parallel polarizer. Actually, the signal through the perpendicular polarizer should be nominally zero in this case but there is some light leakage which provides a background signal level that must be subtracted. The origin of the light leakage will be discussed in Section IVD but is primarily due to birefringent effects of the cavity mirrors. The plots on the right side show the corresponding traces but with an applied field of E=9.87 kV/cm. In this case, the Kerr induced polarization rotation causes phase change between the electric field components parallel and perpendicular to the field, such that more signal is present through the perpendicular analyzer. The larger signal on the perpendicular analyzer with field on relative to field off clearly shows the signal due to the Kerr effect. Because the polarization ellipticity introduced by the Kerr effect is relatively weak, the signal through the parallel polarizer is relatively unchanged. Our measurement approach, as shown in the next sub-section, is to take the ratio of the area of the signal from the perpendicular analyzer to the area of the signal from the parallel analyzer. (From this ratio, we subtract the ratio of the corresponding traces with field off as a means to subtract the background.) In order to confirm that our signals are not due to some form of electromagnetic interference, we have performed a control test where we have positioned the parallel plates slightly away from the sample tube and we have seen no Kerr signal in this case.

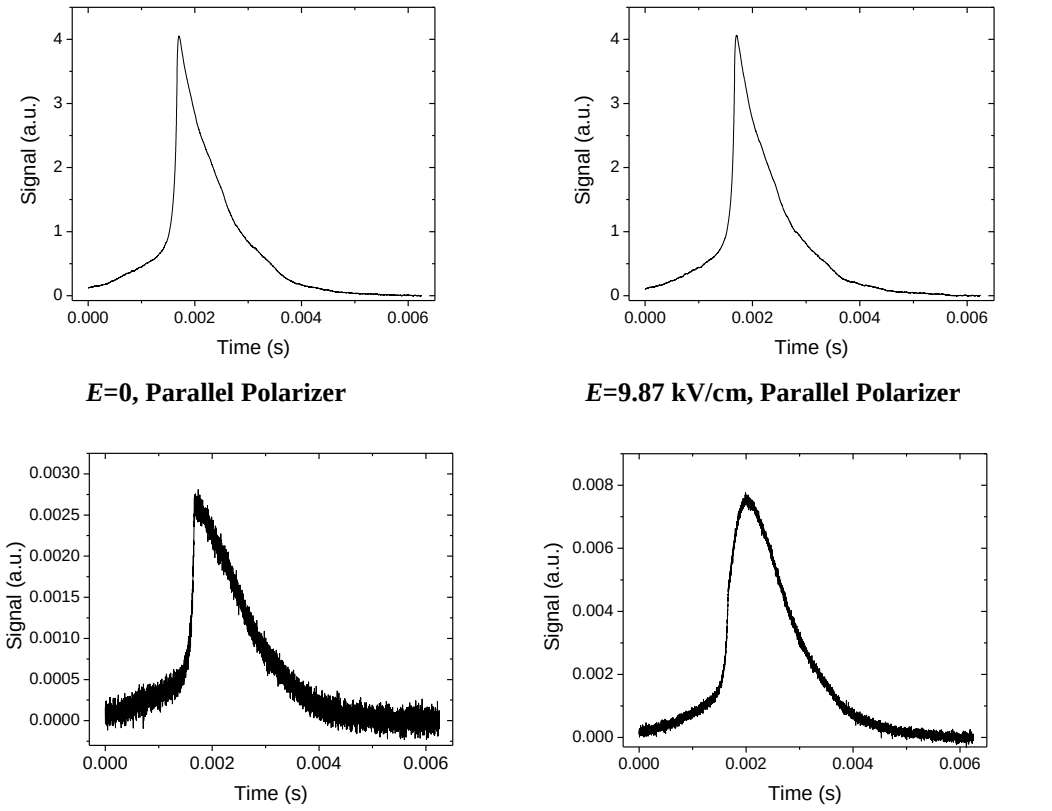

Figure 3. Illustrative Kerr signals due to CO_2 at atmospheric pressure from cavity enhanced polarimeter. Top left: Field off, parallel polarizer. Bottom left: Field off, perpendicular polarizer. Top right: Field on, parallel polarizer. Bottom right: Field on, perpendicular polarizer.

B. Kerr Effect in Different Gases

In this subsection we show polarimeter results for several sample gases and compare against model predictions. Modeling was similar to that discussed in connection with Figure 1. We have simulated the temporal traces for the perpendicular and parallel analyzer orientations and determined the corresponding area ratio. The simulation conditions are as follows: λ=1742 nm, L_0=0.9 m, R=0.999982 (corresponding to τ_{cav} = 166.7 μs and F=174,000), v=4.81μm/s (or equivalent laser scan speed of 5.8 GHz/s though Kerr ratios are quite insensitive to this parameter), and L=0.55 m. The electric fields are computed based on the parallel plate separation, power supply voltage, and correction factor for the dielectric tube (as discussed above). Figure 4 shows experimental results for atmospheric pressure gases of CO_2, N_2, O_2, and air, while Fig. 5 shows CO_2 at pressure of 2.9 atm. The plotted Kerr signal is the ratio of the (temporally integrated) light through the perpendicular polarizer to the light through the parallel polarizer. The background leakage signal has been subtracted from the measurements. For the model, we have used the following wavelength-independent Kerr constants: K_{CO2}=2.08x10^{-24} m^2/V^2 from [11], K_{O2}=4.19x10^{-25} m^2/V^2 from [17] (denoted Carusotto) and K_{O2}=6.58x10^{-25} m^2/V^2 from [11] (denoted Inbar), K_{N2}=1.92x10^{-25} m^2/V^2 from [17] (denoted Carusotto) and K_{N2}=2.65x10^{-25} m^2/V^2 from [11] (denoted Inbar), $K_{air}=0.79K_{N2}+0.21K_{O2}$. The aforementioned values are all for atmospheric pressure (1 atm) and we are assuming a linear scaling for number density and pressure (all measurements are at temperature of 293 K) [14]. The experimental error bars are determined from the system sensitivity and (observed) variation of light leakage level (see below).

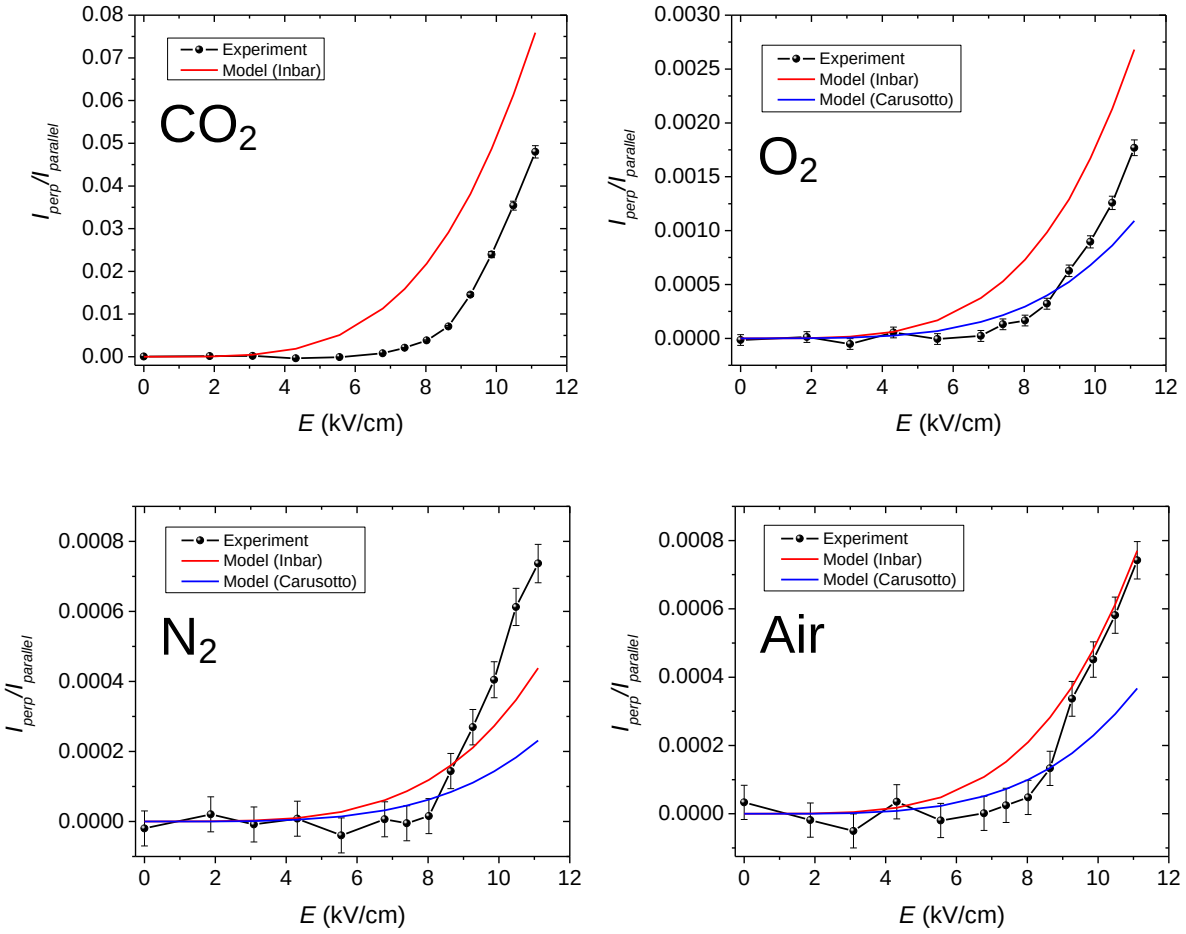

Figure 4. Kerr signal versus applied field for atmospheric pressure CO_2 (top left), O_2 (top right), N_2 (bottom left), and air (bottom right). The Kerr signal is the ratio of the (temporally integrated) light through the perpendicular polarizer to the light through the parallel polarizer.

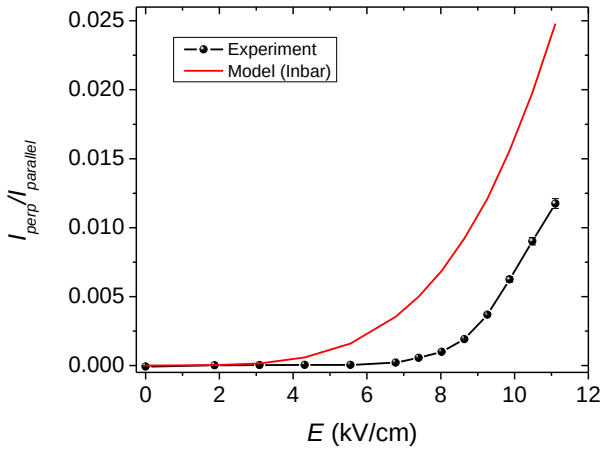

Figure 5. Kerr signal versus applied field for CO_2 at pressure of 2.9 bar. The Kerr signal is the ratio of the (temporally integrated) light through the perpendicular polarizer to the light through the parallel polarizer.

The CO_2 molecule has a large Kerr constant and signal relative to the other gases studied. In our measurement system its signal is evident for fields exceeding ~7 kV/cm. The Kerr constants for N_2 and O_2 are relatively weaker with resulting smaller Kerr signals. The agreement between model and experiment is generally rather good given the uncertainty in the Kerr constants, for example, even for the relatively large constant for CO_2, Inbar et al report an uncertainty of 30% [11] which then becomes consistent with experiment. Another effect, discussed below, that may explain the difference of model versus experiment is laser linewidth effects.

C. Laser Linewidth Effects

Although the linewidth of our DFB laser is relatively small, its effect on the measurements should be considered. It is known that laser linewidth (phase noise) influences the power injection to high-finesse cavities and can alter ring-down and CEAS signals. A particular effect, prevalent when exciting a high-finesse cavity, is that the frequency selective nature of the cavity serves to convert laser phase-noise to power amplitude fluctuations. The amplitude fluctuations, as discussed below, are a limiting factor in the sensitivity of our system. We have also quantitatively examined the effect of laser linewidth on the signals (through the parallel and perpendicular analyzer polarized) in our experiment. For this analysis, we use expressions from Morville et al. that are similar to eqn. (7) but that include random walk due to laser phase noise [18]. (The expressions we use are based on eqn. (12) of the Morville publication though we have fixed an error of inconsistent dimensions.) We have considered cases for N_2 and CO_2 for applied fields of 8.5 kV/cm and we have assumed a (short term) laser linewidth of 100 kHz. For each of the cases we have run 300 simulations (each seeded with different random phase fluctuations) and looked at the mean ratio. We find that, in comparison to eqn. (7) which is for a monochromatic laser, the ratio of the areas due to the perpendicular and parallel signals changes by a fractional value of less than 1 part in 10. However, we have not measured our actual laser linewidth and higher linewidths will give larger signal reductions. This issue should be further considered and is not incorporated within the current analysis.

D. Sensitivity and Detection Limits

The detection limit of our instrument is due to the precision with which we can measure the ratios of the perpendicular to parallel light signals. For our measurement configuration (6000 shot averages) and the case of no applied field, the smallest measurable (change of) signal intensity ratio is ~5×10^{-5} (50 ppm). For example, repeated measurements of the background leakage signal (which we assume to be stable) yield 0.00250 ± 0.00005. A similar conclusion is found by looking at the signal variation for low field conditions in Figure 3. We have verified with our model that, for rough calculations, one can relate the per-pass Kerr phase change to the analyzer intensity ratio by using eqn. (4) and introducing the cavity enhancement factor:

$$I_0 / I_i \approx \sin^2\left(\frac{2F}{\pi}\frac{\theta_K}{2}\right). \tag{8}$$

In this case we use I_0/I_i should be interpreted analogously as the ratio of the light through the perpendicular polarizer to parallel polarizer, i.e. to the quantity plotted on the ordinate axis of Fig. 4 and 5. (In fact, for sufficiently weak birefingence, eqn. (8) gives the correct intensity ratio very accurately if one also introduces a multiplier of 0.5.) Using eqn. (8) with a minimum measurable I_0/I of 5×10^{-5} yields, for our conditions, a minimum measurable per-pass Kerr phase change of 0.2 μradians. In comparison to the work of Kumada et al., who used an optical cell and electrode length of 1.3 m in a 10-pass configuration, we have achieve a lower minimum measurable phase change by a factor of approximately 250. In terms of using our diagnostic for studying plasmas in atmospheric pressure air, the current system allows measurements of fields of E≈7 kV/cm for our 55 cm length electrodes which would correspond to field amplitudes of approximately 15 kV/cm and 50 kV/cm for shorter field lengths of 10 cm and 1 cm respectively. These sensitivities are within range of the field strengths seen in the cathode fall of direct current glow discharges [12, 13], and suggest that this CRDP measurement might be a useful method for probing the field strength in the sheaths of discharge plasmas. Such a diagnostic could be useful in characterizing the field from a wire to plate corona discharge, with the laser propagating along the length of the long wire electrode [19].

More experimental characterization is needed to understand the physical origin of our detection limit. For example, in terms of pure length enhancement, our effective electrode length is ~50 km, which is ~4000 times longer than that of Kumada et al., meaning we could expect roughly another order of magnitude sensitivity improvement. Factors which also play into our sensitivity limit include possible variation in the cavity background birefringence as well as detector noise and shot noise (particularly for the perpendicular analyzer leg) where the optical power is low and we

use an uncooled extended wavelength InGaAs detector. Better performance may be achieved by changing to a lower laser wavelength where more sensitive (regular InGaAs) detectors can be used and, assuming truly wavelength-independent Kerr constants, higher phase shifts arise for given field conditions.

For measurements of very weak phase shifts the birefringent nature of the optical cavity itself should be considered [20]. We have observed that our light leakage signal is due predominantly to the optical cavity and not to the suppression of our polarizers. The observed light leakage of ~0.0025 corresponds to a phase change of ~1 μradians per mirror per pass which is approximately consistent with measured values [20, 21]. If the cavity mirror acts as a pure (and stable) waveplate then, as we have done, its phase contribution can be subtracted as a background, but as discussed by Huang et al. optical cavities can also exhibit linear dichroism (polarization dependent loss). While they may be less useful for practical plasma implementations several recent publications have considered more complex locked and modulated schemes that allow measurements of smaller phase shifts [21, 22].

V. Conclusion

We have developed and demonstrated a new optical diagnostic for measurement of electric fields. The technique uses the Kerr effect and the length enhancement provided by high finesse optical cavities. Demonstrative measurements of electric fields in CO_2, N_2, O_2, and air at atmospheric pressure and with field strengths of several kV/cm (over path lengths of 55 cm) have been shown. Experimental measurements are in reasonable agreement with a model, though laser linewidth effects should be further considered to increase model accuracy. The measurement technique may be useful for studying sheaths of discharge plasmas and wire to plate corona discharges. The cavity enhanced technique provides more than two orders of magnitude improved sensitivity (to phase change) compared to optical Kerr experiments using shorter path lengths.

References

1. Buckingh.Ad; D. A. Dunmur, Transactions of the Faraday Society 64 (547P) (1968) 1776-
2. C. W. Bruce, Physical Review 44 (8) (1933) 0682-0686
3. W. M. Breazeale, Physical Review 48 (3) (1935) 237-240
4. A. Kumada; A. Iwata; K. Ozaki; M. Chiba; K. Hidaka, Journal of Applied Physics 92 (5) (2002) 2875-2879
5. T. Muller; K. B. Wiberg; P. H. Vaccaro, Journal of Physical Chemistry A 104 (25) (2000) 5959-5968
6. T. Muller; K. B. Wiberg; P. H. Vaccaro; J. R. Cheeseman; M. J. Frisch, Journal of the Optical Society of America B-Optical Physics 19 (1) (2002) 125-141
7. R. Engeln; G. Berden; E. vandenBerg; G. Meijer, Journal of Chemical Physics 107 (12) (1997) 4458-4467
8. R. Engeln; G. Berden; R. Peeters; G. Meijer, Review of Scientific Instruments 69 (11) (1998) 3763-3769
9. M. Mansuripur, in: *Optics and Photonics News*, 1998; pp 53-58.
10. F. Bielsa; R. Battesti; C. Robilliard; G. Bialolenker; G. Bailly; G. Trenec; A. Rizzo; C. Rizzo, European Physical Journal D 36 (3) (2005) 261-269
11. E. Inbar; A. Arie, Applied Physics B-Lasers and Optics 70 (6) (2000) 849-852
12. H. Shan; S. A. Self; M. A. Cappelli in: *Optical Emission-Based Measurements of Electric Field in the Cathode Fall Region of He and CF4/He DC Glow Discharges*, 44th Annual Gaseous Electronics Conference, Albuquerque New Mexico, 1991; Albuquerque New Mexico, 1991.
13. Y. W. Choi; M. D. Bowden; K. Muraoka, Applied Physics Letters 69 (10) (1996) 1361-1363
14. D. Chauvat; A. Le Floch; M. Vallet; F. Bretenaker, Applied Physics Letters 73 (8) (1998) 1032-1034
15. F. Brandi; F. Della Valle; P. Micossi; A. M. De Riva; G. Zavattini; F. Perrone; C. Rizzo; G. Ruoso, Journal of the Optical Society of America B-Optical Physics 15 (4) (1998) 1278-1281
16. K. Hidaka; H. Fujita, Journal of Applied Physics 53 (9) (1982) 5999-6003
17. S. Carusotto; E. Iacopini; E. Polacco; F. Scuri; G. Stefanini; E. Zavattini, Nuovo Cimento Della Societa Italiana Di Fisica D-Condensed Matter Atomic Molecular and Chemical Physics Fluids Plasmas Biophysics 5 (4) (1985) 328-338
18. J. Morville; D. Romanini; M. Chenevier; A. Kachanov, Applied Optics 41 (33) (2002) 6980-6990
19. P. Bérard; D. A. Lacoste; C. O. Laux, IEEE TRANSACTIONS ON PLASMA SCIENCE 39 (11) (2011)
20. H. F. Huang; K. K. Lehmann, Applied Optics 47 (21) (2008) 3817-3827
21. M. Durand; J. Morville; D. Romanini, Physical Review A 82 (3) (2010)
22. J. Morville; D. Romanini, Applied Physics B-Lasers and Optics 74 (6) (2002) 495-501